J. Fluid Mech. (1982), *vol.* 118, *pp.* 393–409
Printed in Great Britain

The initial lift and drag of an impulsively started airfoil of finite thickness

By CHUEN-YEN CHOW AND MING-KE HUANG

Department of Aerospace Engineering Sciences, University of Colorado, Boulder, Colorado 80309, USA

(Received 24 August 1981)

The method of apparent masses is utilized to compute the initial lift and drag of an airfoil that starts impulsively from rest. Analytical solutions are obtained for inviscid incompressible flow past a slightly cambered airfoil at a small angle of attack. For a Joukowski airfoil with a cusped trailing edge, it is found that increasing camber or angle of attack will cause increases in both initial lift and drag, whereas increasing thickness will result in an opposite effect. Effects of trailing-edge angle are examined by considering the symmetric Kármán–Trefftz airfoil. The result shows that both lift and drag vanish at the initial instant if the airfoil has a finite trailing-edge angle.

1. Introduction

When an airfoil at an angle of attack starts impulsively from rest, a circulation is generated around the airfoil and a vortex sheet is shed in the wake. The strength of the vortex sheet is determined by requiring that the total circulation of the fluid system be vanishing, and in the meantime the Kutta condition be satisfied at the trailing edge at all times. The problem of a flat-plate airfoil has been solved by Wagner (1925) and by Kármán & Sears (1938), based upon the assumption of an undistorted flat wake sheet. Their results show that the initial lift of the airfoil is one-half of the final steady-state value.

Considering airfoils of finite thickness and allowing wake deformations, Giesing (1968) developed a numerical method for computing the lift on an airfoil of arbitrary shape executing arbitrary unsteady motions. Because of the special computational procedures involving finite time increments, the lift at the initial instant could not be calculated. However, from the lift versus time plots shown in figure 1, Giesing's curve for a 25·5 % thick symmetric Joukowski airfoil (of vanishing trailing-edge angle) and that for an 8·4 % thick symmetric von Mises airfoil (of finite trailing-edge angle) indicate that their lifts seem to reach finite but different initial values as time approaches zero. Basu & Hancock (1978), on the other hand, using much smaller time steps during the initial period and further requiring zero loading across the wake vortex sheet in addition to the Kutta condition on the unsteady airfoil, found that the initial lift of the 8·4 % thick von Mises airfoil tended to zero, as shown in the same figure.

To explain the differences among various solutions that have been displayed in figure 1, a study is needed to examine especially the effects of thickness and trailing-edge angle on the unsteady performance of an airfoil. Numerical methods are inevitable

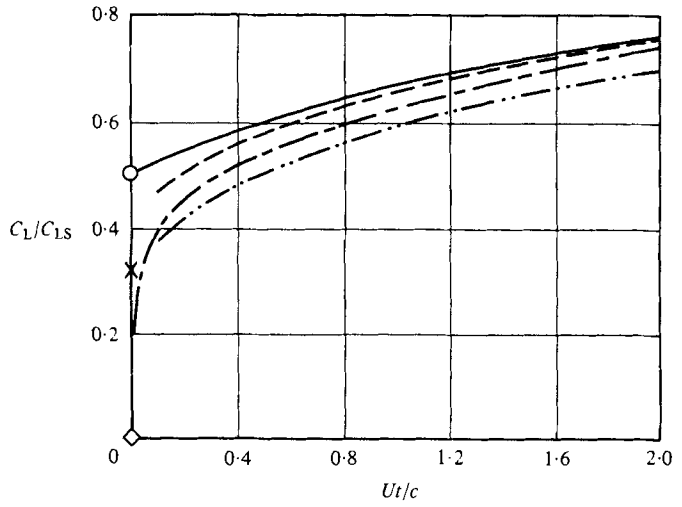

FIGURE 1. Lift coefficient of impulsively started symmetric airfoils at a small angle of attack. Results based upon present method: ○, flat plate; ×, 25·5% thick Joukowski airfoil; ◇, Kármán–Trefftz airfoil of finite trailing-edge angle. ——, flat plate (Wagner 1925); – – –, 8·4% von Mises (Giesing 1968); ·—·, 8·4% von Mises (Basu & Hancock 1978); –··–, 25·5% Joukowski (Giesing 1968).

in such a study. However, if only the solution at the initial instant is to be sought, it will be shown that the results can be expressed in closed form by using the method of apparent masses, which was originated by Jones (1939) for computing the unsteady lift of a wing of finite aspect ratio.

To apply the method to the two-dimensional case, it is assumed, for the initial period immediately following the impulsive motion of an airfoil, that the wake vortex sheet shed from the trailing edge moves with the airfoil as if it were an impermeable extension of the airfoil, while keeping a vanishing total circulation in the flow. The apparent masses of the airfoil–wake combination can be derived as functions of time after the rate of elongation of the wake length is determined from the vortex-shedding velocity. Momenta of the apparent masses are then computed, whose time derivatives should give the unsteady forces exerted on the airfoil. However, at the sharp-turning surfaces of the airfoil where the velocity is infinite (for example at the leading edge of a flat plate and at the tip of the shedding vortex sheet), there exist suctional forces that must also be included in the computation. Since our analysis is restricted to slightly cambered airfoils moving at small angles of attack, these singular forces, which can theoretically be evaluated by taking limiting processes, have higher-order small effects on the lift, and can therefore be ignored. Thus we approximate the lift as the force perpendicular to the chord instead of that perpendicular to the airfoil motion. On the other hand, the drag, whose magnitude is one order smaller than that of the lift, cannot be computed in this manner without including the singular forces; it is evaluated alternatively by balancing the unsteady energy that is also expressed in terms of the apparent masses.

The procedure is illustrated in § 2 to compute the starting lift and drag of a flat-plate airfoil moving suddenly from rest. The result agrees with that of Wagner's analysis at the initial instant. The analysis is then extended to airfoils of finite thickness. Con-

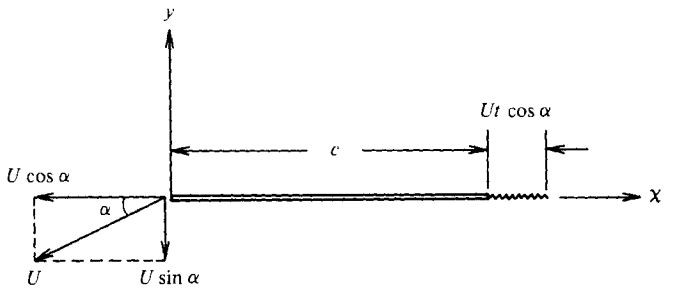

FIGURE 2. Impulsively started flat-plate airfoil.

sidered respectively in §§ 3 and 4 are the Joukowski and Kármán–Trefftz airfoils having respectively vanishing and finite trailing-edge angles. Our results are compared with the initial lift and drag extrapolated from the curves obtained by Giesing and Basu & Hancock, and an explanation of the discrepancy between their numerical solutions is attempted.

2. The flat-plate airfoil

The problem in consideration is sketched in figure 2, showing a thin flat-plate airfoil, of chord c and at an angle of attack α, that has started impulsively from rest with a constant velocity U. Since the airfoil is moving away from its wake at the speed $U\cos\alpha$, we assume that the length of the wake vortex sheet, being shed tangentially from the trailing edge, increases at a fixed rate equal to this speed. This assumption, which automatically fulfils the Kutta condition, is justified mathematically in § 3. Within a short time t after the impulsive start, the wake has a negligibly small deformation, so that it is treated as a short extension of the flat plate. The instantaneous flow is thus equivalent to that generated by moving a rigid plate of length $c + Ut\cos\alpha$ with a normal velocity $U\sin\alpha$.

Let K be the kinetic energy per unit depth of the fluid caused by the motion of a two-dimensional body. It may be expressed as a function of velocities u and v of the body that are respectively in the x- and y-directions:

$$K = \tfrac{1}{2}m_{11}u^2 + m_{12}uv + \tfrac{1}{2}m_{22}v^2, \tag{1}$$

where m_{ij} are the apparent masses associated with the fluid motion, and the relation $m_{21} = m_{12}$ has been used. For the elongated flat plate consisting of the airfoil and wake shown in figure 1, the apparent masses are (Nielsen 1960, p. 371), with ρ denoting the fluid density,

$$m_{11} = 0, \quad m_{12} = 0, \quad m_{22} = \tfrac{1}{4}\pi\rho(c + Ut\cos\alpha)^2, \tag{2}$$

in terms of which the fluid momentum in the y-direction has the expression

$$M_y = -m_{22}U\sin\alpha. \tag{3}$$

The time rate of change of momentum gives the force exerted on the fluid. This force can only be exerted by the solid surface of the airfoil, so that the reaction, or the lift per unit span of the airfoil, is computed from

$$L = -\frac{dM_y}{dt}. \tag{4}$$

As mentioned in § 1, the actual lift is perpendicular to U, so that the preceding equation holds only approximately. The lift coefficient of the airfoil during the starting period is, from (2)–(4),

$$C_{\mathrm{L}} = \frac{L}{\frac{1}{2}\rho U^2 c} = \tfrac{1}{2}\pi \sin 2\alpha \left(1 + \frac{Ut}{c}\cos\alpha\right). \tag{5}$$

By letting t approach zero, we obtain the initial lift coefficient

$$C_{\mathrm{L0}} = \tfrac{1}{2}C_{\mathrm{LS}}, \tag{6}$$

where

$$C_{\mathrm{LS}} = \pi \sin 2\alpha \tag{7}$$

is the steady-state lift coefficient of the flat-plate airfoil, which is usually written as $2\pi\alpha$ for small angles of attack. The result represented by (6) agrees exactly with Wagner's solution.

The drag force is computed from the energy consideration. For the present flow, (1) becomes

$$K = \tfrac{1}{2}m_{22}(U \sin\alpha)^2. \tag{8}$$

Conservation of energy requires that the work done by the drag D per unit time be equal to the rate at which the fluid kinetic energy is increased. Thus we have

$$D = \frac{1}{U}\frac{dK}{dt}. \tag{9}$$

The direction of the drag is opposite to that of U. The drag coefficient is defined in the same way as that shown in (5) for the lift coefficient. After substituting from (2), (8), and (9) and taking the limit, an expression is obtained for the initial drag coefficient,

$$C_{\mathrm{D0}} = \tfrac{1}{2}\pi \sin^2\alpha \cos\alpha. \tag{10}$$

This agrees again with the result $\frac{1}{2}\pi\alpha^2$, deduced from Wagner's function for small α (Garrick 1957, p. 705), as indicated in figure 3.

We have demonstrated that the method of apparent masses predicts correctly the initial lift and drag of a flat plate. This method is relatively simple in that the tedious procedure of determining the strengths of airfoil- and wake-vortex sheets and that of evaluating and integrating the unsteady pressure distribution around the airfoil are avoided. The method is now applied to study the initial behaviour of airfoils of finite thickness.

3. The Joukowski airfoil

Sketched in the physical (x, y)-plane of figure 4(*a*) is an impulsively started Joukowski airfoil whose chord is slightly longer than $4c_1$, c_1 being a characteristic length. The airfoil generally has a camber and its cusped trailing edge makes an angle 2β with the x-axis. Since the trailing-edge angle vanishes, the appropriate Kutta condition is that the fluid velocity V_t at the trailing edge be finite and be tangent to the local airfoil surface. At an instant t shortly after the impulsive start, a vortex sheet of length $\Delta(= V_t t)$ is shed in the wake, making an angle 2β with the x-axis. In analogy to the flat-plate problem, the initial lift and drag are determined from the apparent masses of a body consisting of both the airfoil and the wake.

According to a general method described by Nielsen (1960), the apparent masses of

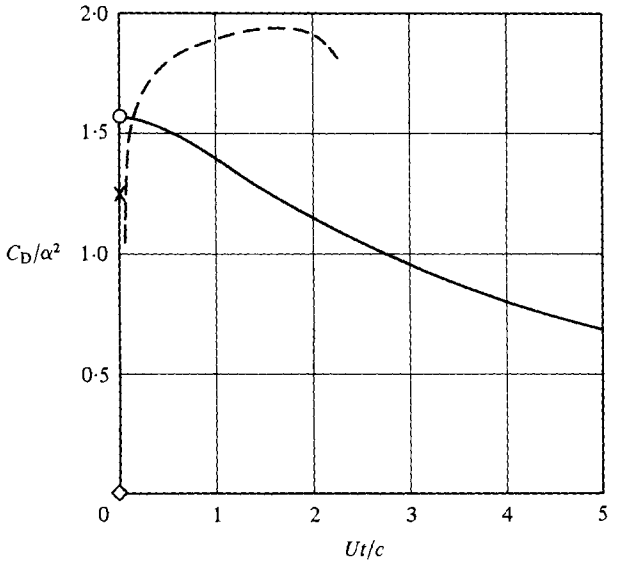

FIGURE 3. Drag coefficient of impulsively started symmetric airfoils at a small angle of attack. Results based upon present method: ○, flat plate; ×, 25·5% thick Joukowski airfoil; ◇, Kármán–Trefftz airfoil of finite trailing-edge angle. ——, flat plate (Garrick 1957); – – –, 8·4% von Mises (Basu & Hancock 1978).

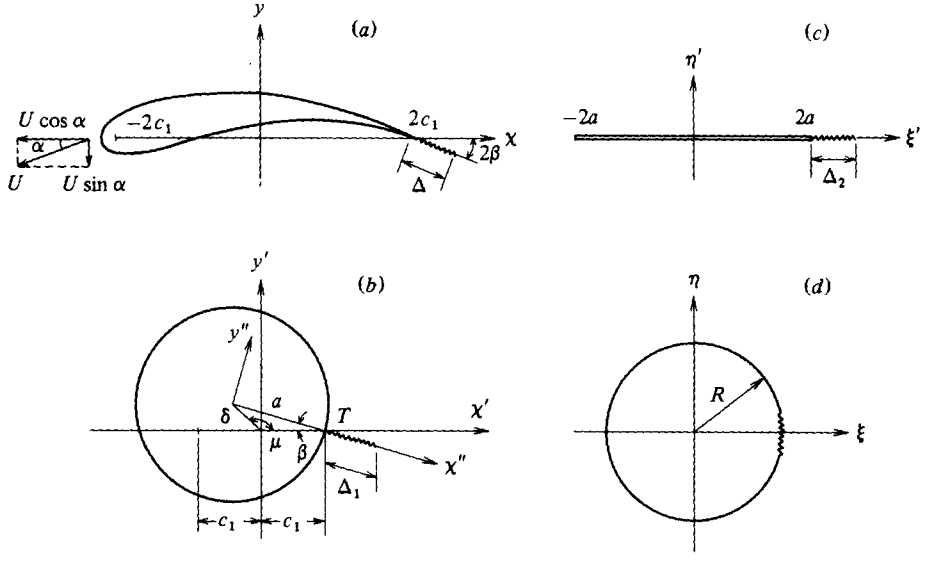

FIGURE 4. Successive transformations of a Joukowski airfoil and its wake into a circle. (*a*) ($z = x+iy$)-plane; (*b*) ($z' = x'+iy'$)- and ($z'' = x''+iy''$)-planes; (*c*) $\zeta' = (\xi'+i\eta')$-plane; (*d*) ($\zeta = \xi+i\eta$)-plane.

any two-dimensional body are immediately obtained if the body contour can be mapped into a circle. Let us first map the airfoil into a circle of radius a in the z'-plane as shown in figure 4(*b*) through the Joukowski transformation

$$z = z' + \frac{c_1^2}{z'}, \tag{11}$$

in which $z = x + iy$ and $z' = x' + iy'$. The trailing edge of the airfoil is mapped into the point T at $z' = c_1$, and the wake vortex sheet is mapped into a radial line segment passing through T if the length of the vortex sheet is infinitesimal. The airfoil geometry is generated by specifying the two shape parameters δ and μ defined in figure 4 (*b*). The radius of the circle

$$a = (c_1^2 + \delta^2 - 2c_1\delta\cos\mu)^{\frac{1}{2}} \tag{12}$$

determines the chord, and the angle

$$\beta = \arctan\frac{\delta\sin\mu}{1-\delta\cos\mu} \tag{13}$$

determines the orientation of the trailing edge.

The flow around the airfoil can be obtained by transforming that around the circle in the z'-plane, which consists of a uniform flow U at an angle of attack α, a doublet of strength Ua^2 at the centre of the circle, a bound vortex of circulation Γ about the circle, and a flow induced by the wake vortex sheet. The Kutta condition when applied in the z'-plane requires that the resultant flow speed be zero at the point T. It can be proved in a straightforward manner that any point vortex on the wake vortex sheet and its image inside the circle will modify the magnitude of Γ in order to keep T a stagnation point, but they will not change either the magnitude or the orientation of the velocity V_t at the airfoil trailing edge. Thus, as long as the vortex sheet is on the radial line through T, vortices are shed at the velocity

$$V_t = U\frac{c_1}{a}\cos(\alpha+\beta) \tag{14}$$

in a direction that makes a clockwise angle of 2β with the x-axis. The classical result of (14) can be found, for example, in Kármán & Burgers (1943).

The flat plate is a special case of the Joukowski airfoil generated by letting $\delta = 0$. This gives $a = c_1$ and $\beta = 0$, so that $V_t = U\cos\alpha$, which justifies the vortex-shedding velocity assumed in § 2 for the flat plate based on an intuitive argument.

From (14), the length of the vortex sheet trailing behind the Joukowski airfoil is calculated:

$$\Delta = Ut\frac{c_1}{a}\cos(\alpha+\beta). \tag{15}$$

To find the length Δ_1 of the sheet in the z'-plane, the transformation (11) in the neighbourhood of the trailing edge is approximated by

$$z' - c_1 \simeq [(z-2c_1)\,c_1]^{\frac{1}{2}}.$$

It maps the tip of the vortex sheet at $z = 2c_1 + \Delta e^{-i2\beta}$ into a point at $z' = c_1 + (c_1\Delta)^{\frac{1}{2}}e^{-i\beta}$, so that

$$\Delta_1 = (c_1\Delta)^{\frac{1}{2}}. \tag{16}$$

The co-ordinate system is shifted to the centre of the circle and in the meantime is rotated through an angle β, as shown in figure 4 (*b*), by the transformation

$$z'' = (z' - \delta e^{i\mu})\,e^{i\beta}. \tag{17}$$

A further transformation

$$\zeta' = z'' + \frac{a^2}{z''} \tag{18}$$

maps the circle into a flat plate of length $4a$ and the vortex sheet into an extended line segment of length Δ_2 (see figure 4*c*). The size of the wake in the ζ'-plane can be determined by considering the approximation of (18) in the neighbourhood of the trailing edge:

$$\zeta' - 2a \simeq \frac{(z''-a)^2}{a}.$$

Mapping of the tip of the vortex sheet yields $\Delta_2 = \Delta_1^2/a$, or, from (16),

$$\Delta_2 = \frac{c_1}{a}\Delta. \tag{19}$$

The combination of the horizontal plate and wake in the ζ'-plane is finally mapped into a circle of radius R in the ζ-plane of figure 4(*d*) by the transformation

$$\zeta' - \tfrac{1}{2}\Delta_2 = \zeta + \frac{R^2}{\zeta}, \tag{20}$$

where

$$R = a + \tfrac{1}{4}\Delta_2. \tag{21}$$

The successive transformations (11), (17), (18) and (20) can be summarized in the form of a single transformation

$$z = \zeta e^{-i\beta} + \sum_{n=0}^{\infty} \frac{a_n}{(\zeta e^{-i\beta})^n}, \tag{22}$$

in which, in particular,

$$a_1 = c_1^2 + (R^2 - a^2)\, e^{-i2\beta}. \tag{23}$$

Coefficients other than a_1 are not needed in the computation for apparent masses. The derivation of (22) and (23) is given in appendix A.

The apparent masses are functions of R, a_1 and the cross-sectional area S of the airfoil. According to Nielsen (1960),

$$m_{11} = 2\pi\rho\left[R^2 - \frac{S}{2\pi} - \mathscr{R}(a_1)\right], \tag{24a}$$

$$m_{12} = -2\pi\rho\mathscr{I}(a_1), \tag{24b}$$

$$m_{22} = 2\pi\rho\left[R^2 - \frac{S}{2\pi} + \mathscr{R}(a_1)\right], \tag{24c}$$

in which $\mathscr{R}$ and $\mathscr{I}$ indicate respectively the real and imaginary parts. With $\Delta/a \ll 1$ in (19), expressions (21) and (23) can be approximated by

$$R^2 \simeq a^2 + \tfrac{1}{2}c_1\Delta, \quad a_1 \simeq c_1^2 + \tfrac{1}{2}c_1\Delta e^{-i2\beta}.$$

Thus for the Joukowski airfoil with a very short wake, the apparent masses are

$$m_{11} = M_{11} + \pi\rho c_1\Delta(1 - \cos 2\beta), \tag{25a}$$

$$m_{12} = \pi\rho c_1\Delta \sin 2\beta, \tag{25b}$$

$$m_{22} = M_{22} + \pi\rho c_1\Delta(1 + \cos 2\beta), \tag{25c}$$

where

$$M_{11} = 2\pi\rho\left(a^2 - \frac{S}{2\pi} - c_1^2\right), \tag{25d}$$

$$M_{22} = 2\pi\rho\left(a^2 - \frac{S}{2\pi} + c_1^2\right) \tag{25e}$$

are the apparent masses of the airfoil without a wake.

The momentum and kinetic energy of the flow shown in figure 4(*a*) are respectively

$$M_y = -m_{12} U \cos\alpha - m_{22} U \sin\alpha, \tag{26}$$

$$K = \tfrac{1}{2} m_{11} (U\cos\alpha)^2 + m_{12} U^2 \sin\alpha\cos\alpha + \tfrac{1}{2} m_{22} (U\sin\alpha)^2. \tag{27}$$

Substituting (25) into (26) and (27), with Δ expressed as a function of t by (15), and then performing time differentiations according to (4) and (9), we obtain the starting lift and drag after letting $t \to 0$. They have the following forms:

$$L_0 = \frac{1}{a} \pi c_1^2 \rho U^2 \cos\beta \sin 2(\alpha+\beta), \tag{28}$$

$$D_0 = \frac{1}{2a} \pi c_1^2 \rho U^2 \sin(\alpha+\beta) \sin 2(\alpha+\beta). \tag{29}$$

Effects of airfoil geometry on initial lift and drag are examined separately. The right-hand sides of (28) and (29) indicate that airfoil camber and angle of attack have the same effect of increasing both the initial lift and drag. The influence of thickness can be found by considering the approximated relationship for thin airfoils of small camber (Pope 1951, p. 97) that

$$\frac{a}{c_1} \simeq 1 + 0{\cdot}77 \frac{d}{c}, \tag{30}$$

where d/c is the maximum-thickness to chord ratio. Upon substitution from (30), (28) and (29) show that both lift and drag become smaller at the initial instant for a thicker airfoil.

The steady-state lift of the Joukowski airfoil is (Kármán & Burgers 1943)

$$L_S = 4\pi a \rho U^2 \sin(\alpha+\beta), \tag{31}$$

whose ratio to (28) yields

$$\frac{C_{L0}}{C_{LS}} = \frac{L_0}{L_S} = \frac{1}{2} \left(\frac{c_1}{a}\right)^2 \cos\beta \cos(\alpha+\beta). \tag{32}$$

This equation enables us to determine the missing initial value of the lift-ratio versus time curve, obtained numerically by Giesing (1968) for the 25·5 % thick symmetrical Joukowski airfoil, plotted in figure 1. Since the approximate expression (30) holds only for thin airfoils, the ratio a/c_1 is determined alternatively by assigning different values to δ in (12) with $\mu = \pi$ and then observing the corresponding airfoil shapes. The value $a/c_1 = 1{\cdot}25$ is thus obtained for this particular airfoil. For $\beta = 0$ and for a small angle of attack, (32) gives $C_{L0}/C_{LS} = 0{\cdot}32$, which is represented by a cross on the vertical axis of figure 1. It is interesting to note that an extension of Giesing's curve for that airfoil would go right through this crossed point, just like the case of a flat plate in which the Wagner's curve passes through the circled point obtained by using the method of apparent masses.

For a flat plate, c_1/a becomes unity, and (32) reduces to (6) within the approximation of small angles.

Non-dimensionalizing (29) based upon a chord of length $c \simeq 4c_1$, we obtain an expression for the initial drag coefficient that

$$C_{D0} = \frac{\pi c_1}{4a} \sin(\alpha+\beta) \sin 2(\alpha+\beta), \tag{33}$$

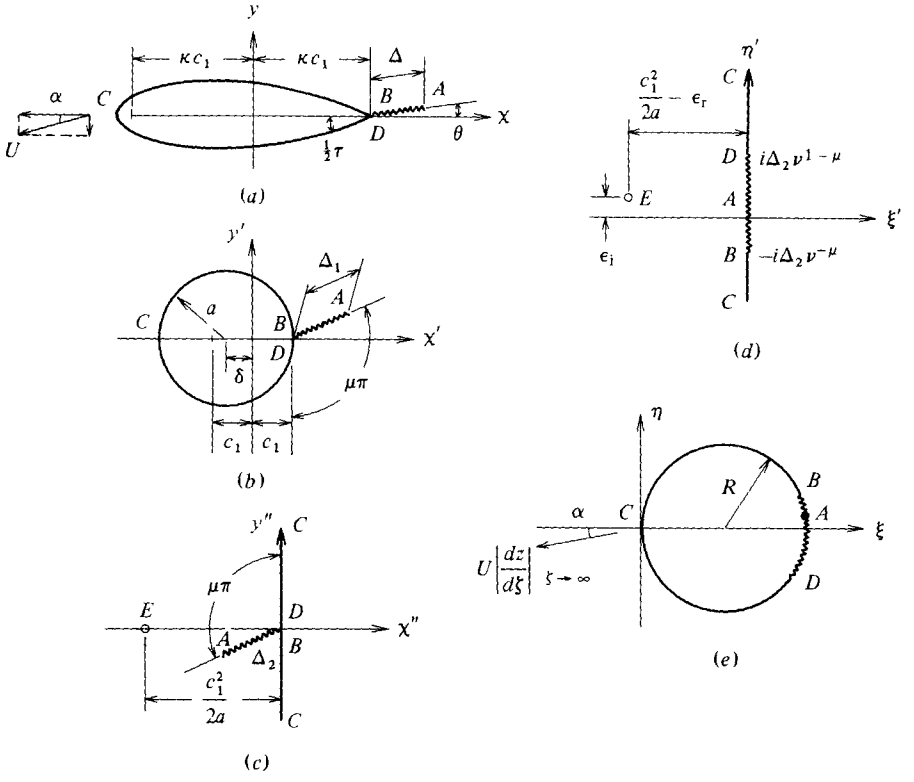

FIGURE 5. Successive transformations of a Kármán–Trefftz airfoil and its wake into a circle. (*a*) $(z = x+iy)$-plane; (*b*) $(z' = x'+iy')$-plane; (*c*) $(z'' = x''+iy'')$-plane; (*d*) $(\zeta' = \xi'+i\eta')$-plane; (*e*) $(\zeta = \xi+i\eta)$-plane.

which reduces to (10) for the flat-plate airfoil. This formula gives $C_{D0}/\alpha^2 = 1{\cdot}256$ for the 25·5 % thick symmetrical Joukowski airfoil moving at a small angle of attack. The result is represented by a cross in figure 3.

If we let the circle shown in figure 4(*b*) be centred on the y'-axis so that $c_1/a = \cos\beta$, the resulting equations (28) and (29) become the expressions for the starting lift and drag of an infinitely thin airfoil having the shape of a circular arc.

4. The Kármán–Trefftz airfoil

We now consider an airfoil that, unlike the cusped Joukowski airfoil, has a finite trailing-edge angle. Because of its well-known conformal-mapping properties, the uncambered Kármán–Trefftz airfoil is chosen as the object of our analyses. Such an airfoil, having a trailing-edge angle τ, is sketched in the physical z-plane of figure 5(*a*). It is mapped into a circle in the z'-plane as shown in figure 5(*b*) through the transformation (Kármán & Burgers 1943, chap. 2)

$$\frac{z-\kappa c_1}{z+\kappa c_1} = \left(\frac{z'-c_1}{z'+c_1}\right)^{\kappa}, \tag{34}$$

where

$$\kappa = 2-\tau/\pi. \tag{34a}$$

The circle passes through the point $z' = c_1$ with its centre on the negative x'-axis at a distance δ from the origin. The radius $a(= c_1 + \delta)$ controls the shape of the airfoil, whose trailing edge is always at $z = \kappa c_1$. The Joukowski transformation (11) is a special case of (34) with $\tau = 0$.

Suppose the airfoil has a short wake of length Δ making an angle θ with the x-axis. The transformation (34) maps the wake into a straight line of length Δ_1 that makes an angle $\mu\pi$ with the negative y'-axis, where

$$\Delta_1 = \left[(2c_1)^{\kappa-1}\frac{\Delta}{\kappa}\right]^{1/\kappa}, \tag{35}$$

$$\mu\pi = \tfrac{1}{2}\pi + \frac{\theta}{\kappa}. \tag{36}$$

Again, in order to compute the apparent masses, transformations must be found that successively map the airfoil and its wake into a circle. They are first transformed from the z'-plane into the z''-plane according to the relationship

$$z'' = \frac{c_1^2}{z' + a + \delta} - \frac{c_1^2}{2a}, \tag{37}$$

so that the airfoil maps into the entire y''-axis, and the wake becomes a line segment of length Δ_2 as shown in figure 5(*c*). This transformation consequently maps the entire region at infinity into the point E on the negative x''-axis. It can easily be shown that

$$\Delta_2 = \left(\frac{c_1}{2a}\right)^2 \Delta_1. \tag{38}$$

The airfoil–wake combination is further mapped into the vertical axis of the ζ'-plane in figure 5(*d*) by the transformation

$$z'' = (\zeta' - i\Delta_2 \nu^{1-\mu})^{\mu} (\zeta' + i\Delta_2 \nu^{-\mu})^{1-\mu}, \tag{39}$$

in which

$$\nu = \frac{\mu}{1-\mu}. \tag{40}$$

For a very small Δ_2, (39) causes the position of E to change slightly from $-c_1^2/2a$ in the z''-plane to $-c_1^2/2a + \epsilon$ in the ζ'-plane, where $\epsilon = \epsilon_r + i\epsilon_i$ is a small complex perturbation quantity with

$$\epsilon_r = \mu(1-\mu)\frac{a\Delta_2^2}{c_1^2}(\nu^{1-\mu} + \nu^{-\mu})^2, \tag{41}$$

$$\epsilon_i = \Delta_2[\mu\nu^{1-\mu} - (1-\mu)\nu^{-\mu}], \tag{42}$$

which are obtained after neglecting terms of order of Δ_2^3 or higher.

Finally, the airfoil and its wake are mapped as shown in figure 5(*e*) into a circle of radius

$$R = \frac{ac_1^2}{c_1^2 - 2a\epsilon_r}, \tag{43}$$

and the point E is mapped back to infinity in the ζ-plane by the transformation

$$\zeta = \frac{c_1^2}{\zeta' + c_1^2/2a - \epsilon}. \tag{44}$$

With details given in appendix B, we combine transformations (34), (37), (39) and (44) into a compact form

$$z = \zeta \Big/ \frac{c_1^2}{2a}\left(\frac{\mu}{P}+\frac{1-\mu}{Q}\right) + \sum_{n=0}^{\infty} a_n \left[\zeta \Big/ \frac{c_1^2}{2a}\left(\frac{\mu}{P}+\frac{1-\mu}{Q}\right)\right]^{-n}, \tag{45}$$

in which

$$P = \frac{c_1^2}{2a} - \epsilon + i\Delta_2 \nu^{1-\mu}, \tag{46}$$

$$Q = \frac{c_1^2}{2a} - \epsilon - i\Delta_2 \nu^{-\mu}, \tag{47}$$

$$a_1 = \tfrac{1}{3}(\kappa^2-1)\, c_1^2 + 8\left(\frac{a}{c_1}\right)^4 \mu(1-\mu)\,(\nu^{1-\mu}+\nu^{-\mu})^2\, \Delta_2^2. \tag{48}$$

We can now proceed to compute the apparent masses for the airfoil–wake combination. It turns out for a symmetric airfoil that m_{12} vanishes and m_{11} is not influenced by the wake and therefore is not a function of time. Because $dz/d\zeta \neq 1$ as $\zeta \to \infty$, the expression (24*c*) for m_{22} is modified to read

$$m_{22} = 2\pi\rho\left[\left(R\left|\frac{dz}{d\zeta}\right|_{\zeta\to\infty}\right)^2 - \frac{S}{2\pi} + \mathscr{R}(a_1)\right]. \tag{49}$$

It gives, upon substitution from (43), (45), and (48) and then using (35) and (38),

$$m_{22} = M_{22} + 2\pi\rho\nu^{1-2\mu}\left[\frac{(2c_1)^{\kappa-1}\Delta}{\kappa}\right]^{2/\kappa}, \tag{50}$$

in which

$$M_{22} = 2\pi\rho\left(a^2 - \frac{S}{2\pi} + \tfrac{1}{3}(\kappa^2-1)\, c_1^2\right) \tag{51}$$

is the expression for the airfoil without a wake. Note that a, S, and c_1 defined in figure 5 for the Kármán–Trefftz airfoil are different from those defined in figure 4 for the Joukowski airfoil.

To check the correctness of the above analyses, let us consider a special case in which $\tau = 0$ (vanishing trailing-edge angle) and $\theta = 0$ (horizontal wake), so that $\kappa = 2, \mu = \frac{1}{2}$, and $\nu = 1$. With these values, (50) and (51) correspond respectively to (25*c*) and (25*e*), after letting $\beta = 0$ for an uncambered Joukowski airfoil.

The next task is to find an expression for the wake length Δ in (50) as a function of time. According to our model, the airfoil and its initial wake move together like a rigid body, with the circulation about the airfoil equal but opposite to that about the wake vortex sheet. The Kármán–Trefftz airfoil, unlike the flat plate or the Joukowski airfoil, has a vanishing velocity at the trailing edge so that its vortex-shedding velocity cannot be computed in the previous manner. On the other hand, at the free end of the wake vortex sheet, which is designated A in figure 5(*a*), the velocity becomes unbounded. We consider the rate at which the vortex sheet elongates as the average of the velocities at two points that are immediately above and below the sheet at point A. With details shown in appendix C, we obtain

$$\frac{d\Delta}{dt} = f U \Delta^{(2-\kappa)/\kappa}, \tag{52}$$

with
$$f = \frac{2\cos\alpha}{a}(2c_1)^{2(\kappa-1)/\kappa}\kappa^{-(\kappa+2)/\kappa}\nu^{1-2\mu}. \tag{53}$$

Integration of (52) yields the desired expression for the wake length that
$$\Delta = \left[\frac{2(\kappa-1)}{\kappa}fUt\right]^{\kappa/2(\kappa-1)}. \tag{54}$$

Let us take a closer look at the function f. The right-hand side of (53) is determined by the geometry of the airfoil and the angle of attack; except for the last group, which is determined instead by ν and μ. Since ν is related to μ through (40), and μ itself is a function of θ as shown by (36), that group in (53) describes the influence of the orientation of the wake vortex sheet. More explicitly, upon substituting ν from (40) and κ from (34a), (53) and (36) can respectively be rewritten as
$$f \propto \left(\frac{1-\mu}{\mu}\right)^{2\mu-1}, \tag{55}$$
$$\mu = \tfrac{1}{2} + \frac{\frac{1}{2}\theta}{\pi - \frac{1}{2}\tau}. \tag{56}$$

Keeping airfoil geometry and angle of attack the same, these relations show that f has a maximum at, and is symmetric about, $\theta = 0$, and that f decreases continuously toward zero as the magnitude of θ increases toward its maximum value of $\pi - \frac{1}{2}\tau$. See figure 5(a) for a geometric interpretation of the preceding statement.

Fluid kinetic energy is obtained after substituting (54) into (50) and then into (27), noting that $m_{12} = 0$ and m_{11} is a constant. Its unsteady part is found to be proportional to f raised to a constant power, so that, from the property of f, the kinetic energy has a maximum at $\theta = 0$ and decreases with increasing magnitude of θ. However, the wake-orientation angle is restricted by the Kutta condition. For $|\theta| < \frac{1}{2}\tau$ the flow at the trailing edge turns through an angle that is deflected into the oncoming flow on either the upper or the lower surface of the airfoil; both points B and D in figure 5(a) are therefore stagnation points. For $\theta > \frac{1}{2}\tau$, the flow on the lower surface turns through an angle deflecting away from the original flow direction, causing an infinite velocity at point D, in violation of the Kutta condition. Similarly the Kutta condition is not satisfied at point B if $\theta < -\frac{1}{2}\tau$. When $\theta = \frac{1}{2}\tau$, the wake vortex sheet is tangent to the lower surface of the airfoil at the trailing edge, so that the velocity at D is finite and that at B vanishes. The situation is reversed if $\theta = -\frac{1}{2}\tau$. It is thus concluded that the possible values of θ are those within the range $-\frac{1}{2}\tau \leqslant \theta \leqslant \frac{1}{2}\tau$.

In order to narrow down that range further, we argue that the actual flow must be the one that causes least kinetic energy in the fluid. This requirement results in two possible values, $\theta = \pm\frac{1}{2}\tau$, from the result of the kinetic-energy analysis. The physical difference between these two cases is that when $\theta = \frac{1}{2}\tau$ the shed vorticity is counterclockwise, whereas when $\theta = -\frac{1}{2}\tau$ it is clockwise and is therefore in the same direction as that of the circulation around the airfoil. These two cases have been sketched by Basu & Hancock (1978) in their figure 4. The latter case is eliminated on the ground that the total circulation around a path enclosing both the airfoil and wake must be zero. The final result for the orientation of shed vortex sheet that $\theta = \frac{1}{2}\tau$ agrees with that obtained by Basu & Hancock demanding a zero pressure difference on the upper

$\frac{Ut}{a}$	$\frac{C_L}{C_{LS}}\left(\frac{c_1}{a}\right)^{-2}$		
	$\tau/\pi = 0{\cdot}05$	$\tau/\pi = 0{\cdot}1$	$\tau/\pi = 0{\cdot}2$
0	0	0	0
10^{-6}	0·258	0·134	0·036
10^{-5}	0·290	0·168	0·057
10^{-4}	0·325	0·212	0·090
10^{-3}	0·365	0·267	0·142
10^{-2}	0·410	0·336	0·225
10^{-1}	0·460	0·423	0·357

TABLE 1. Time variation of lift coefficient of Kármán–Trefftz airfoils of various trailing-edge angles during the early stage of an impulsive motion

and lower surfaces at the trailing edge, and also with that obtained by Giesing (1969) requiring a smooth flow there. Substitution of this particular value of θ into (56) yields

$$\mu = \frac{1}{2-\tau/\pi}, \tag{57}$$

which simplifies (40) to

$$\nu = \frac{1}{1-\tau/\pi}. \tag{58}$$

We are now ready to compute the unsteady lift. Substituting (54) into (50) and then into (26), and then performing differentiation according to (4), we obtain

$$L = \frac{8\pi}{a}\rho U^2 c_1^2 \sin\alpha \left[4\cos\alpha\,\kappa^{-4}\,\nu^{\kappa(1-2\mu)}\left(\frac{Ut}{a}\right)^{2-\kappa}\right]^{1/(\kappa-1)}. \tag{59}$$

The steady lift of the symmetric Kármán–Trefftz airfoil is, as shown in Kármán & Burgers (1943),

$$L_S = 4\pi\rho U^2 a \sin\alpha. \tag{60}$$

After use of (34a), (57), and (58), the ratio of (59) and (60) gives

$$\frac{C_L}{C_{LS}} = 2\left(\frac{c_1}{a}\right)^2\left[4\cos\alpha\left(2-\frac{\tau}{\pi}\right)^{-4}\left(1-\frac{\tau}{\pi}\right)^{\tau/\pi}\left(\frac{Ut}{a}\right)^{\tau/\pi}\right]^{1/(1-\tau/\pi)}. \tag{61}$$

The airfoil becomes a symmetric Joukowski airfoil when the trailing-edge angle τ vanishes. In such a case (61) reduces to (32) with $\beta = 0$, so that the initial lift is finite. On the other hand, the initial lift vanishes for any finite value of τ, as represented by a point at the origin in figure 1.

For small angles of attack we let $\cos\alpha \simeq 1$ in (61) and examine the effect of trailing-edge angle by computing the time variation of $(C_L/C_{LS})/(c_1/a)^2$ for three non-vanishing values of τ. The result displayed in table 1 shows that lift increases very rapidly at a rate which decreases with increasing τ. Since a thicker airfoil has a smaller c_1/a ratio, the pick-up rate is therefore slower for such an airfoil.

A direct comparison of our analytical result for the Kármán–Trefftz airfoil with the numerical results, plotted in figure 1, obtained by Giesing and Basu & Hancock for an 8·4 % thick von Mises airfoil, is not possible. However, the lift curve by Basu & Hancock behaves in the same way as that predicted by our theory. The large discrepancy between this and Giesing's curve, which seems to approach a non-vanishing

value as $t \to 0$, is most likely caused by the relatively large time steps used in Giesing's numerical procedure.

The unsteady drag, computed by using (8) and (9), is proportional to dm_{22}/dt and thus is proportional to the expression contained in the square brackets on the right-hand side of (61). The result that the initial drag vanishes for an airfoil of finite trailing-edge angle is represented in figure 3. Basu & Hancock's drag curve for the von Mises airfoil seems to conform with our theoretical prediction.

5. Conclusion

We have demonstrated that analytical solutions for the starting performance can be obtained for various airfoils, as long as the airfoil and its short wake can be mapped into a circle. Our result for the cusped Joukowski airfoil reveals that increasing camber or angle of attack will raise the initial lift and drag, whereas increasing thickness will cause an opposite effect. The influence of trailing-edge angle is studied by considering the symmetrical Kármán–Trefftz airfoil. It is found that any finite trailing-edge angle causes both lift and drag to decrease to zero at the starting instant of the impulsive motion. The rate of increase of initial lift decreases with increasing either trailing-edge angle or thickness. In other words, a thicker airfoil or an airfoil with a larger trailing-edge angle exhibits a higher resistance to lift increase.

Our analysis holds only for a very short period immediately after the motion is started, because the assumption of a straight wake soon becomes invalid when the free end of the shed vortex sheet starts to roll into a spiral.

The analysis can be extended to accommodate large α and β angles by including suctional forces exerted on all sharp corners at which the velocity becomes infinite. With additional mathematical manipulations, a more general analysis can be carried out for a cambered Kármán–Trefftz airfoil. However, we expect that the effects of camber are analogous to those found for the cambered Joukowski airfoil.

This work was supported by the Air Force Office of Scientific Research under Grant No. AFOSR 81-0037, administered by Michael S. Francis.

Appendix A. Derivation of (22) and (23)

Solving (17) for z' and substituting the result into (11) yields

$$z = z'' e^{-i\beta} + \delta e^{i\mu} + \frac{c_1^2 e^{i\beta}}{z''} - \frac{c_1^2 \delta e^{i(2\beta+\mu)}}{z''^2} + \dots \tag{A 1}$$

for small δ/z''. Now from (18), and then using (20),

$$\begin{aligned} z'' &= \tfrac{1}{2}\zeta' \left[1 + \left(1 - 4\frac{a^2}{\zeta'^2}\right)^{\frac{1}{2}}\right] \\ &= \zeta' - \frac{a^2}{\zeta'} + \dots \\ &= \zeta + \tfrac{1}{2}\Delta_2 + \frac{R^2}{\zeta} - \frac{a^2}{\zeta}\left(1 + \frac{\Delta_2}{2\zeta} + \frac{R^2}{\zeta^2}\right)^{-1} + \dots \\ &= \zeta + \tfrac{1}{2}\Delta_2 + \frac{R^2 - a^2}{\zeta} + \dots . \end{aligned} \tag{A 2}$$

Substitution of z'' from (A 2) into (A 1) gives

$$z = \left(\zeta + \tfrac{1}{2}\Delta_2 + \frac{R^2-a^2}{\zeta} + \ldots\right) e^{-i\beta} + \delta e^{i\mu} + \frac{c_1^2}{\zeta e^{-i\beta}}\left(1 + \frac{\Delta_2}{2\zeta} + \frac{R^2-a^2}{\zeta^2} + \ldots\right)^{-1} + \ldots$$

$$= \zeta e^{-i\beta} + (\tfrac{1}{2}\Delta_2 e^{-i\beta} + \delta e^{i\mu}) + \frac{c_1^2 + (R^2-a^2)\, e^{-i2\beta}}{\zeta e^{-i\beta}} + \ldots$$

$$= \zeta e^{-i\beta} + \sum_{n=0}^{\infty} \frac{a_n}{(\zeta e^{-i\beta})^n}, \tag{22}$$

in which a_1 has the expression described by (23).

Appendix B. Derivation of (45) and (48)

ζ' is first expressed in terms of ζ by using (44). The expression is then substituted into (39) to give

$$z'' = \left(\frac{c_1^2}{\zeta} - \frac{c_1^2}{2a} + \epsilon - i\Delta_2 \nu^{1-\mu}\right)^{\mu} \left(\frac{c_1^2}{\zeta} - \frac{c_1^2}{2a} + \epsilon + i\Delta_2 \nu^{-\mu}\right)^{1-\mu}$$

$$= -P^{\mu} Q^{1-\mu} \left(1 - \frac{c_1^2}{P\zeta}\right)^{\mu} \left(1 - \frac{c_1^2}{Q\zeta}\right)^{1-\mu}, \tag{B 1}$$

in which P and Q are defined respectively in (46) and (47). Since z'' has the value of $-c_1^2/2a$ as $\zeta \to \infty$ (see figure 5c), we have

$$P^{\mu} Q^{1-\mu} = \frac{c_1^2}{2a},$$

so that (B 1) becomes

$$z'' = -\frac{c_1^2}{2a}\left[1 - \left(\frac{\mu}{P} + \frac{1-\mu}{Q}\right)\frac{c_1^2}{\zeta} + \mu(1-\mu)\left(\frac{1}{PQ} - \frac{1}{2P^2} - \frac{1}{2Q^2}\right)\frac{c_1^4}{\zeta^2} + \ldots\right]. \tag{B 2}$$

The transformation (34) can be written in the form of an infinite series (Kármán & Burgers 1943, p. 74)

$$z = z' + \tfrac{1}{3}(\kappa^2 - 1)\frac{c_1^2}{z'} + \ldots, \tag{B 3}$$

in which z' is expressed as a function of z'' by using (37):

$$z' = \frac{c_1^2}{z'' + c_1^2/2a} - (a + \delta). \tag{B 4}$$

After substituting (B 2) into (B 4) and then into (B 3), its right-hand side becomes a power series in ζ, as shown in (45). Only the coefficient a_1 in this series affects the apparent masses. It has the form

$$a_1 = \tfrac{1}{3}(\kappa^2 - 1)\, c_1^2 + \mu(1-\mu)\left\{\tfrac{1}{4}\mu(1-\mu)\left(\frac{1}{P} - \frac{1}{Q}\right)^4 \Big/ \left(\frac{\mu}{P} + \frac{1-\mu}{Q}\right)\right.$$

$$\left. + \frac{1}{6}\left[\mu\left(\frac{1}{P} - \frac{1}{Q}\right)^3 + \frac{3}{P^2 Q} - \frac{2}{P^3} - \frac{1}{Q^3}\right]\right\} \Big/ \frac{1}{(2a)^2}\left(\frac{\mu}{P} + \frac{1-\mu}{Q}\right)^3. \tag{B 5}$$

Substituting P and Q from (46) and (47), in which ϵ is defined by (41) and (42), and then expanding the right-hand side of (B 5) as an infinite series in Δ_2, we obtain (48) by retaining terms up to $O(\Delta_2^2)$.

Appendix C. Derivation of (52) and (53)

Let us use subscripts u and ℓ to denote, respectively, the conditions at points immediately above and below the wake vortex sheet at the tip A. If V represents the speed tangent to the sheet and W represents the complex potential of the flow, the rate at which the vortex sheet elongates can be computed,

$$\begin{aligned}\frac{d\Delta}{dt} &= \tfrac{1}{2}(V_{\mathrm{u}}+V_{\ell}) \\ &= \frac{1}{2}\left\{\mathscr{R}\left[\left(\frac{dW}{dz}\right)_{\mathrm{u}} e^{i\theta}\right]_{z_{\mathrm{u}}\to z_A} + \mathscr{R}\left[\left(\frac{dW}{dz}\right)_{\ell} e^{i\theta}\right]_{z_{\ell}\to z_A}\right\} \\ &= \tfrac{1}{2}\mathscr{R}\left\{\left[\left(\frac{dW}{d\zeta}\Big/\frac{dz}{d\zeta}\right)_{\mathrm{u}} e^{i\theta}\right]_{z_{\mathrm{u}}\to z_A} + \left[\left(\frac{dW}{d\zeta}\Big/\frac{dz}{d\zeta}\right)_{\ell} e^{i\theta}\right]_{z_{\ell}\to z_A}\right\}. \end{aligned} \tag{C 1}$$

Expansion about A gives

$$\left(\frac{dW}{d\zeta}\right)_{\mathrm{u}} = \left(\frac{dW}{d\zeta}\right)_A + \left(\frac{d^2W}{d\zeta^2}\right)_A (\zeta_{\mathrm{u}}-\zeta_A)+\ldots, \tag{C 2}$$

$$\left(\frac{dW}{\partial\zeta}\right)_{\ell} = \left(\frac{dW}{d\zeta}\right)_A + \left(\frac{d^2W}{d\zeta}\right)_A (\zeta_{\ell}-\zeta_A)+\ldots, \tag{C 3}$$

$$\left(\frac{dz}{d\zeta}\right)_{\mathrm{u}} = \left(\frac{dz}{d\zeta}\right)_A + \left(\frac{d^2z}{d\zeta^2}\right)_A (\zeta_{\mathrm{u}}-\zeta_A)+\ldots, \tag{C 4}$$

$$\left(\frac{dz}{d\zeta}\right)_{\ell} = \left(\frac{dz}{d\zeta}\right)_A + \left(\frac{d^2z}{d\zeta^2}\right)_A (\zeta_{\ell}-\zeta_A)+\ldots, \tag{C 5}$$

in which $(dz/d\zeta)_A$ can be shown to be zero.

Referring to figure 5(*e*), we let ω be the angle between the ξ-axis and the radius of the circle passing through A. It is assumed that, after being mapped into the ζ-plane, those two points above and below the vortex sheet become points on the opposite sides of that radius, so that

$$\zeta_{\mathrm{u}}-\zeta_A = \lambda\, e^{i(\omega+\frac{1}{2}\pi)}, \tag{C 6}$$

$$\begin{aligned}\zeta_{\ell}-\zeta_A &= \lambda\, e^{i(\omega-\frac{1}{2}\pi)} \\ &= -\lambda\, e^{i(\omega+\frac{1}{2}\pi)},\end{aligned} \tag{C 7}$$

where λ is an infinitesimal distance. Substituting (C 2–C 7) into (C 1), we obtain

$$\frac{d\Delta}{dt} = \mathscr{R}\left[\left(\frac{d^2W}{d\zeta^2}\right)_A e^{i\theta}\Big/\left(\frac{d^2z}{d\zeta^2}\right)_A\right]. \tag{C 8}$$

It is not difficult to show, by virtue of the fact that point A is in the close vicinity of the airfoil trailing edge, that

$$\left(\frac{d^2z}{d\zeta^2}\right)_A = e^{i\theta}\nu^{2\mu-1}[(2c_1)^{2(1-\kappa)}\kappa^{\kappa+2}\Delta^{\kappa-2}]^{1/\kappa}. \tag{C 9}$$

The complex potential of the flow about the circle shown in figure 5(*e*) of vanishing circulation is

$$W = U\left|\frac{dz}{d\zeta}\right|_{\zeta\to\infty} e^{-i\alpha}\left(\zeta-R+\frac{R^2e^{i2\alpha}}{\zeta-R}\right),$$

from which we obtain

$$\left(\frac{d^2W}{d\zeta^2}\right)_A = \frac{2U}{a}e^{i\alpha}, \tag{C 10}$$

after using the approximations that $(dz/d\zeta)_{\zeta\to\infty} \simeq 1$ and $R \simeq a$, and the fact that point A is at an infinitesimal distance above the ξ-axis. Substitution of (C 9) and (C 10) into (C 8) yields (52) and (53).

REFERENCES

Basu, B. C. & Hancock, G. J. 1978 The unsteady motion of a two-dimensional aerofoil in incompressible inviscid flow. *J. Fluid Mech.* **87**, 159–178.

Garrick, I. E. 1957 Non-steady wing characteristics. *High Speed Aerodynamics and Jet Propulsion*, vol. VII, section F. Princeton University Press.

Giesing, J. P. 1968 Nonlinear two-dimensional unsteady potential flow with lift. *J. Aircraft* **5**, 135–143.

Giesing, J. P. 1969 Vorticity and Kutta condition for unsteady multienergy flows. *Trans. A.S.M.E.* E, *J. Appl. Mech.* **91**, 608–613.

Jones, R. T. 1939 The unsteady lift of a wing of finite aspect ratio. *NACA Rep.* no. 681.

Kármán, T. von & Burgers, J. M. 1943 General aerodynamic theory – perfect fluids. *Aerodynamic Theory*, vol. II, division E. Durand Reprinting Committee, California Institute of Technology.

Kármán, T. von & Sears, W. R. 1938 Airfoil theory for non-uniform motion. *J. Aero. Sci.* **5** 6–17.

Nielsen, J. N. 1960 *Missile Aerodynamics*. McGraw-Hill.

Pope, A. 1951 *Basic Wing and Airfoil Theory*. McGraw-Hill.

Wagner, H. 1925 Über die Entstehung des dynamischen Auftriebes von Tragflügeln. *Z. angew. Math. Mech.* **5**, 17–35.